

# Self-administered transcranial direct current stimulation treatment of knee osteoarthritis alters pain-related fNIRS connectivity networks

Samuel Montero-Hernandez<sup>✉,a</sup>, Luca Pollonini<sup>b,c,d</sup>, Lindsey Park,<sup>e</sup>, Geraldine Martorella<sup>e</sup>, Hongyu Miao<sup>e</sup>, Kenneth B. Mathis,<sup>f</sup> and Hyochol Ahn<sup>e</sup>

<sup>a</sup>University of Houston, Department of Engineering Technology, Houston, Texas, United States

<sup>b</sup>University of Houston, Department of Electrical and Computer Engineering, Houston, Texas, United States

<sup>c</sup>University of Houston, Department of Biomedical Engineering, Houston, Texas, United States

<sup>d</sup>Basque Center on Cognition, Brain and Language, San Sebastian, Spain

<sup>e</sup>Florida State University, College of Nursing, Tallahassee, Florida, United States

<sup>f</sup>The University of Texas Health Science Center at Houston, McGovern Medical School, Department of Orthopedic Surgery, Houston, Texas, United States

## Abstract

**Significance:** Knee osteoarthritis (OA) is a disease that causes chronic pain in the elderly population. Currently, OA is mainly treated pharmacologically with analgesics, although research has shown that neuromodulation via transcranial direct current stimulation (tDCS) may be beneficial in reducing pain in clinical settings. However, no studies have reported the effects of home-based self-administered tDCS on functional brain networks in older adults with knee OA.

**Aim:** We used functional near-infrared spectroscopy (fNIRS) to investigate the functional connectivity effects of tDCS on underlying pain processing mechanisms at the central nervous level in older adults with knee OA.

**Approach:** Pain-related brain connectivity networks were extracted using fNIRS at baseline and for three consecutive weeks of treatment from 120 subjects randomly assigned to two groups undergoing active tDCS and sham tDCS.

**Results:** Our results showed that the tDCS intervention significantly modulated pain-related connectivity correlation only in the group receiving active treatment. We also found that only the active treatment group showed a significantly reduced number and strength of functional connections evoked during nociception in the prefrontal cortex, primary motor (M1), and primary somatosensory (S1) cortices. To our knowledge, this is the first study in which the effect of tDCS on pain-related connectivity networks is investigated using fNIRS.

**Conclusions:** fNIRS-based functional connectivity can be effectively used to investigate neural circuits of pain at the cortical level in association with nonpharmacological, self-administered tDCS treatment.

© The Authors. Published by SPIE under a Creative Commons Attribution 4.0 International License. Distribution or reproduction of this work in whole or in part requires full attribution of the original publication, including its DOI. [DOI: [10.1117/1.NPh.10.1.015011](https://doi.org/10.1117/1.NPh.10.1.015011)]

**Keywords:** transcranial direct current stimulation; functional connectivity; pain; knee osteoarthritis; neuromodulation.

Paper 22093GR received Sep. 30, 2022; accepted for publication Mar. 7, 2023; published online Mar. 31, 2023.

---

\*Address all correspondence to Samuel Montero-Hernandez, [smonteroherandez@uh.edu](mailto:smonteroherandez@uh.edu)

## 1 Introduction

Knee osteoarthritis (OA) is a degenerative condition that destroys the cartilage inside the joint, resulting in persistent pain and functional changes, such as swelling and stiffness. It is one of the main causes of pain and physical disability in adults, affecting over 14 million people in the United States alone and millions more worldwide.<sup>1,2</sup> Although knee OA can manifest at any age, it is predominant in aging adults over 50 years old, especially women.<sup>3</sup>

Pain caused by knee OA is mainly treated with pharmacologic agents, often producing significant adverse effects.<sup>4,5</sup> Among alternative or complementary nonpharmacological approaches for pain management caused by knee OA, transcranial direct current stimulation (tDCS) has gathered interest due to its safety, noninvasiveness, and efficacy in pain reduction.<sup>6-8</sup> Briefly, tDCS consists of passing a low-intensity electrical direct current between two electrodes placed on the scalp for a certain duration of time (e.g., typically 20 min) in an attempt to promote neuronal excitability within neuronal pain networks.<sup>9</sup>

Our research has previously shown that tDCS has a beneficial effect on clinical subjective measures of pain in knee OA patients,<sup>10</sup> as well as experimental pain sensitivity.<sup>11,12</sup> We reported the efficacy of home-based tDCS treatment on experimental pain sensitivity measures such as the heat pain threshold (HPT<sub>h</sub>), heat pain tolerance (HPT<sub>t</sub>), pressure pain threshold (PPT), and conditioned pain modulation (CPM), as well as its relationship with clinical pain intensity measures such as the numeric rating scale (NRS) and Western Ontario and McMaster Universities Osteoarthritis Index. Changes in NPT<sub>h</sub>, NPT<sub>t</sub>, PPT, CPM, and NRS between the active and sham groups were found to be statistically significant after the third week of treatment<sup>12</sup> and 3 months from the baseline.<sup>10</sup> Additionally, we found significant associations between NRS and HPT<sub>h</sub>, NRS and HPT<sub>t</sub>, and NRS and PPT. Furthermore, our group has assessed longitudinal changes in cortical hemodynamics of the tDCS treatment for pain management in a pilot study<sup>13</sup> and showed the benefits of combining tDCS and mindfulness-based meditation.<sup>14,15</sup> However, the mechanistic action of this neuromodulatory approach still needs to be better understood, and the use of neuroimaging offers enormous possibilities to identify the neural basis of pain perception.<sup>16-19</sup>

Among neuroimaging techniques, functional near-infrared spectroscopy (fNIRS) is a non-invasive optical sensing technique that measures cortical hemodynamics and that has been demonstrated to be a good fit for interrogating the brain during and after tDCS sessions.<sup>20</sup> As opposed to functional magnetic resonance imaging, fNIRS bears the advantages of portability and low cost that make it particularly apt for large-sample studies carried out in nonclinical settings.

The study of pain processing with the use of fNIRS has been addressed in different works mostly focused on acute pain conditions, including but not limited to dental pain,<sup>21-23</sup> induced pain in surgery,<sup>24,25</sup> and acupuncture settings pain.<sup>26</sup> Moreover, a growing body of literature reports nonclinical experimental studies employing thermal,<sup>27-30</sup> mechanical,<sup>28,31</sup> and electrical<sup>32-36</sup> pain stimulation. Detailed information about approaches and experimental designs to investigate pain using fNIRS can be found in reviews published by Hu et al.<sup>37</sup> and Peng et al.<sup>38</sup> Although numerous fNIRS studies have explored pain-evoked brain hemodynamics, only a few of them have looked at the potential disruption of functional connectivity induced by pain. In addition, considering that pain mechanisms involve different brain areas,<sup>17,39</sup> no investigations to our knowledge have analyzed the brain connectivity patterns produced by tDCS as a non-pharmacological pain treatment. For instance, Rojas et al.<sup>26</sup> investigated the functional connectivity changes in 11 subjects while monitoring S1 and M1 regions during the insertion, twirl, and removal of acupuncture needles. In another work, Hu et al.<sup>21</sup> explored the evolution of the resting state functional connectivity in the bilateral prefrontal cortex (PFC) and S1 in 12 patients with dentin hypersensitivity before, during, and after cold stimulation to the affected teeth. Finally, Kodama et al.<sup>40</sup> analyzed the analgesic effect of the compression of myofascial trigger points on the connectivity networks recovered from the PFC with a multimodal fNIRS-EEG approach. However, none of these studies involved the use of tDCS as an alternative treatment for pain management.

According to Peyron et al.,<sup>18,19</sup> neuroimaging studies focused on nociception can be divided into five categories: (i) descriptive studies aimed at the identification of patterns of brain regions

involved in the processing of pain, (ii) empathy studies that explore the brain activity in the presence of unpleasant situations, (iii) clinical pain studies investigating the structural and functional brain abnormalities in clinical settings, (iv) modulation of pain studies aimed at the identification of brain regions capable of mediating the pain sensation, and (v) brain connectivity and studies focused on capturing the dynamic mechanisms of pain in terms of network analysis. Following this classification, our work can be considered to be the intersection of categories (iii), (iv), and (v).

In this study, we investigated the cross-sectional and longitudinal effects of a series of fifteen 20-min-long sessions of tDCS on functional brain connectivity in elderly individuals affected by knee OA. To our knowledge, this is the first study assessing changes in neural connections assessed using fNIRS between cohorts that underwent home-based, self-administered tDCS treatment versus sham tDCS for several weeks, and it pairs with other reports from our group focused on clinical outcomes.<sup>10,12–15,41–43</sup>

## 2 Materials and Methods

### 2.1 Participants

For this study, we recruited a total of 120 subjects (84 females,  $66 \pm 8.3$  years) suffering from knee OA. Participants were considered eligible if they had self-reported unilateral or bilateral knee OA pain, according to the American College of Rheumatology criteria.<sup>44</sup> Nine subjects did not complete the study. The detailed protocol and enrollment procedures are described in our previous article reporting the primary outcomes of our study.<sup>10</sup>

Exclusion criteria included a history of brain surgery, brain tumor, seizure, stroke, or intracranial metal implantation; uncontrolled hypertension, heart failure, or myocardial infarction; alcohol/substance abuse; cognitive impairment; and a history of psychiatric illness. The study protocol was approved by the UTHealth Institutional Review Board prior to commencement and is registered with ClinicalTrials.gov (NCT04016272), and participants signed an informed consent form. Each participant was trained in the use of a portable tDCS device ( $1 \times 1$  tDCS Soterix Inc., New York, United States) to self-administer a 20-min tDCS session using 2 mA for 3 weeks (Monday to Friday) at home or a private room. The tDCS device consisted of two  $5 \times 7$  cm electrodes, with the anode placed over the primary motor cortex M1 (contralateral to the affected knee) and the cathode covering the supraorbital area SO (ipsilateral to the painful knee). Participants were randomly assigned to either an active treatment or a sham group in a 1:1 ratio. For the active stimulation, the participant received a 2-mA constant direct current for 20 min according to the anode-cathode placement described before, whereas the sham group only received the electrical current stimulation for 30 s at the beginning and end of the session, with no direct current stimulation for the rest of the time. All sessions were monitored through a secure video conference platform (e.g., WebEx) to ensure that the proper brain stimulation technique was used and to monitor any adverse events.

### 2.2 Pain Experimental Protocol and fNIRS Data Collection

Functional connectivity was investigated by recording fNIRS signals during knee-localized thermal stimulation and, on a subset of participants, punctate pain stimulation. Thermal pain stimulation was applied via a commercially available thermal sensory testing machine (Medoc, Inc.) and delivered through a small thermal probe ( $1 \times 1$  in.) applied to the affected knee. Additionally, mechanical punctate stimulation was applied using a commercially available hand-held probe (North Coast Medical, Inc.). All subjects received thermal pain stimulation, whereas only 89 received both thermal and punctate stimulation. The experimental block design consisted of applying pain stimulation for 20 s in six repetitions interleaved with resting periods of 30 s.

Pain-related brain responses were monitored using fNIRS at baseline (i.e., prior to any tDCS session) and after completing the first, second, and third weeks of treatment. The fNIRS device (LightNIRS, Shimadzu, Japan) consisted of eight light sources (semiconductor lasers at 780, 805, and 830 nm) and eight detectors arranged in a grid-like layout covering the PFC and

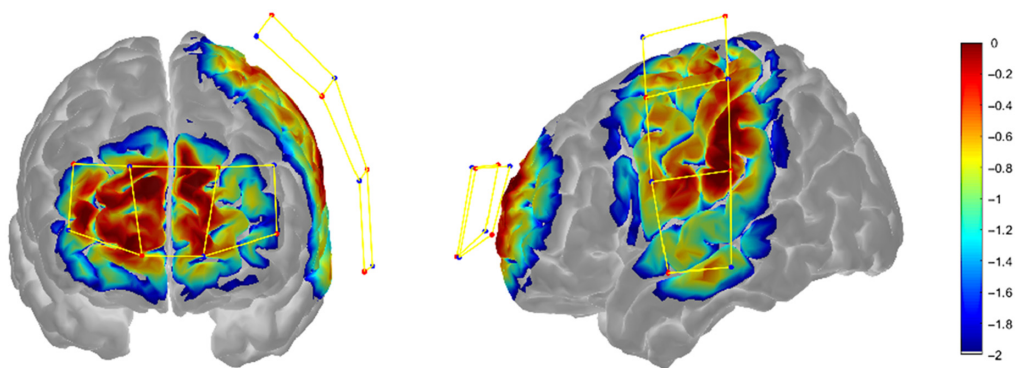


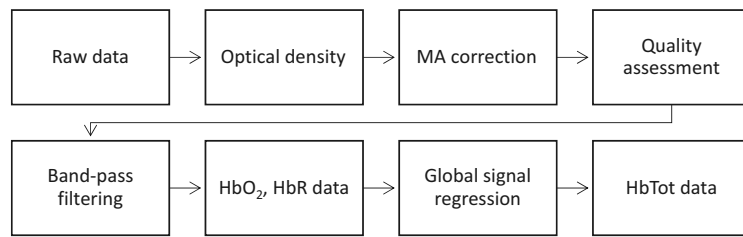
**Fig. 1** Sensitivity map of the prefrontal region and left hemisphere overlaid onto the Colin27 brain model. Sources, detectors, and channels are depicted as red circles, blue circles, and yellow bar links, respectively. The sensitivity profile was computed and displayed with AtlasViewer.

primary motor (M1) and primary somatosensory (S1) contralateral to the affected knee (Fig. 1). This configuration allowed for measuring the hemodynamic activity with 20 optical channels with a source-detector distance of 30 mm approximately at 13.33 Hz.

### 2.3 Preprocessing of fNIRS Recordings

Prior to fNIRS data analysis, nine subjects were discarded because they withdrew from the study or only completed the baseline (week 0) session. Initial processing of the fNIRS data included the conversion from raw voltage to optical densities and the identification and correction of motion artifacts using the spline interpolation method.<sup>45</sup> To identify recordings with poor quality data, we applied a quality control analysis on each optical channel via the QT-NIRS toolbox<sup>46</sup> using the following parameters:  $SCI_{threshold} = 0.8$ ,  $PSP_{threshold} = 0.1$ , and  $CQS_{threshold} = 75\%$ . Briefly, the scalp coupling index (SCI) and power spectrum peak (PSP) quantify the strength of the cardiac pulse detectable in a short-timed fNIRS signal (e.g., 3 to 5 s) in an optical channel, and the channel quality score (CQS) represents the time fraction of the entire recording that must have sufficient quality to consider such an optical channel acceptable. Unlike activation analyses in which each channel is associated with an activation value (e.g., a statistical  $p$ - or  $q$ -value), functional connectivity analysis is based on the statistical relationship between pairs of channels. Although pruning low-quality channels may make group-level analysis and interpretation challenging because of heterogeneous connectivity matrices across subjects (i.e., networks with a different set of nodes), discarding noisy scans in their entirety improves the quality of the data sets without compromising the feasibility of subsequent analytical steps. For this reason, instead of pruning individual channels with low quality (i.e.,  $CQS < 75\%$ ), we opted to remove entire scans with fewer than five acceptable channels, as they contributed less than minimally to the functional connectivity analysis. Potential concerns arising from the inclusion of individual noisy channels are alleviated by the use of a robust correlation method<sup>47</sup> (described later), which in turn is inspired by the robust regression method called autoregressive (AR) modeling using iteratively reweighted least squares (AR-IRLS).<sup>48</sup> In addition, the quality metrics used in QT-NIRS have been shown to be good indicators of the performance of AR-IRLS.<sup>49</sup>

After data quality evaluation, we applied band-pass filtering (0.01 to 0.2 Hz) to remove undesired components and then converted the data to oxy-hemoglobin ( $HbO_2$ ) and deoxy-hemoglobin (HbR). We then removed the remaining systemic noise by regressing out the mean response across channels for each Hb data type and scan (i.e., global system regression).<sup>50-52</sup> This last step was performed due to the lack of short-separation channels in the fNIRS equipment. Finally, we computed the total hemoglobin (HbT) as the addition of the  $HbO_2$  and HbR. The entire processing pipeline is illustrated in Fig. 2. Data quality assessment was performed using QT-NIRS,<sup>53</sup> and the rest of preprocessing, functional connectivity, and functional activation analyses were conducted using Brain AnalyzIR<sup>54</sup> and Homer 2<sup>55</sup> toolboxes and custom scripts in MATLAB v2021b.

**Fig. 2** Processing pipeline of fNIRS data.

## 2.4 Functional Connectivity Analysis

The brain connectivity analysis typically includes the extraction and representation of the functional connectivity networks. Extraction of the connectivity networks has been done through time-domain methods (correlation or seed-based analysis) or frequency-domain approaches (partial direct coherence or wavelet-based).<sup>56</sup> The network representation approaches include graph theory methods, connectivity matrices, and atlas-based correlation maps, among others.<sup>57</sup> However, both extraction and representation methods have different implications in terms of the type of retrieved information and the statistical analysis procedures. Thus, we chose the extraction and representation methods in function of the change in brain integration given the treatments (active versus sham) and the pain stimuli. From the Hb data, we computed the correlation among fNIRS channels using an AR prewhitening approach, which converts the time-series fNIRS signals to meet the statistical assumptions (independent noise terms and zero autocorrelation).<sup>47</sup> Then we computed the Pearson correlation coefficients for each pair of channels across Hb types and subjects. The correlation was computed from the blocks of pain stimulation, that is, only considering each of the six 20-s trials of the stimulation periods (~120 s). In this sense, the correlation value from channels A and B can be understood as the strength of signal association between those channels while the subject is exposed to the pain stimulation. The group-level analysis was performed over the *R*-coefficients using a linear mixed-effects model considering the group-week interaction for each pain stimulation type. In fNIRS connectivity, the selection of which Hb connectivity network to analyze has been debated. In this case, the similarity between the HbO<sub>2</sub> and HbR networks may assist in determining whether to use either HbO<sub>2</sub> or HbR (when the similarity is high) for the posterior analysis or present the results combining both Hb types. There exist specific metrics to quantify the similarity of connectivity networks; these include the graph edit distance, structural Hamming distance, and differential symmetry index (DSI).<sup>58</sup> We opted to use the DSI to determine the similarity between the HbO<sub>2</sub> and HbR networks because it removes the mathematical contribution of network density that increases the rate of spurious symmetry levels. Once the Hb connectivity network to be used was determined, we estimated the probability density functions (PDFs) from the distribution of the correlation values. The PDFs were computed for each stimulation type and group across weeks to quantify how different or similar the set of functional connections between the sham and active groups were. We employed a kernel density estimation with Gaussian kernels for the density estimation. The similarity between distributions densities was computed by the Hellinger distance.<sup>59,60</sup> For discrete distributions, the Hellinger distance (also known as Jeffreys distance) between two distributions *P* and *Q* is defined as  $H(P, Q) = \frac{1}{\sqrt{2}} \|\sqrt{P} - \sqrt{Q}\|_2$ , where  $\|\cdot\|_2$  denotes the Euclidean norm. We selected the Hellinger distance because it satisfies the axioms of a metric (identity, symmetry, and triangle equality) and generates values in the [0, 1] range, which simplify its interpretation.

To investigate the changes in connectivity at the regional level, we extracted the correlation values at intra- and interregional levels for PFC and primary motor and sensorimotor areas. The regional connectivity was obtained through a subnetwork analysis. First, we obtained the corresponding *t* values from the correlation values through the expression  $t = \frac{r}{S.E.}$ , where  $S.E. = \sqrt{\frac{1-r^2}{n-2}}$  and *n* is the sample size. Then the statistical significance was computed and corrected using a Benjamini–Hochberg correction.

## 2.5 Statistical Analysis at the Subnetwork Level

Statistically, we analyzed functional connectivity both within and between brain regions in an attempt to gain insight into the role of subnetworks involved in functional organization patterns in pain management. Specifically, we described the regional connectivity using mean correlation and mean node degree of subnetworks. The mean correlation represents the strength of connectivity, whereas the mean node degree represents the total wiring cost of a subnetwork.<sup>61</sup> In functional connectivity networks, the division into subnetworks can be done according to different criteria, for instance, anatomical divisions, channels density coverage, and well-known brain circuitry, among others.<sup>62,63</sup> Here we choose a trade-off between the regions of interest relevant to this study and the channel density coverage of our fNIRS setup, thus exploring connectivity in two regions: the PFC and the lateral region that includes the primary motor cortex (M1) and primary sensorimotor (S1) area. We applied the statistical analysis on both measures according to the following scheme. First, the Shapiro–Wilk test was used to examine the normality assumption of data distribution, and then two sample *t*-tests or Wilcoxon Rank sum tests (when normality was not met) were used to compare the active group with the sham group.

## 3 Results

### 3.1 Data Quality

Our approach to data quality evaluation (i.e., triaging scans with less than five acceptable channels) resulted in the exclusion of 56 out of 799 recordings (or 7% of the total) from further processing. The resulting CQS averaged across the screened dataset is shown in Fig. 3. Expectedly, optical channels over the PFC had a visibly higher quality (~95%) compared with those probing the primary motor and somatosensory cortical areas (~60%), where hair obtrusion contributed to an overall lower signal quality.

### 3.2 Time Series

In addition to the quality assessment, the removal of the global systemic signals unveils the hemodynamic changes while discarding the effects of physiology from the scalp when subjects are exposed to pain stimulation. Figure 4 shows the block-averaged HbO<sub>2</sub>, HbR, and HbT group-level responses.

After removing the global systemic components, hemodynamic changes were expectedly observed in the transition from resting to stimulation periods. Increases in HbT were observed on channels covering the motor and somatosensory regions, whereas negative HbT changes took place on channels covering the PFC. In other words, the signals from channels covering the PFC

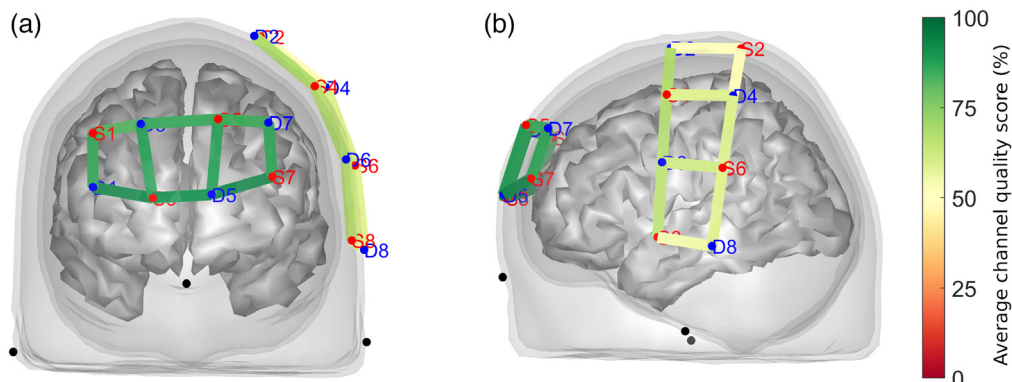


**Fig. 3** Resulting data quality assessment using QT-NIRS after triaging excessively noisy scans. Optical channels covering (a) the prefrontal region exhibited higher quality (CQS close to 95%) than channels over (b) the sensory-motor brain area (CQS close to 60%).

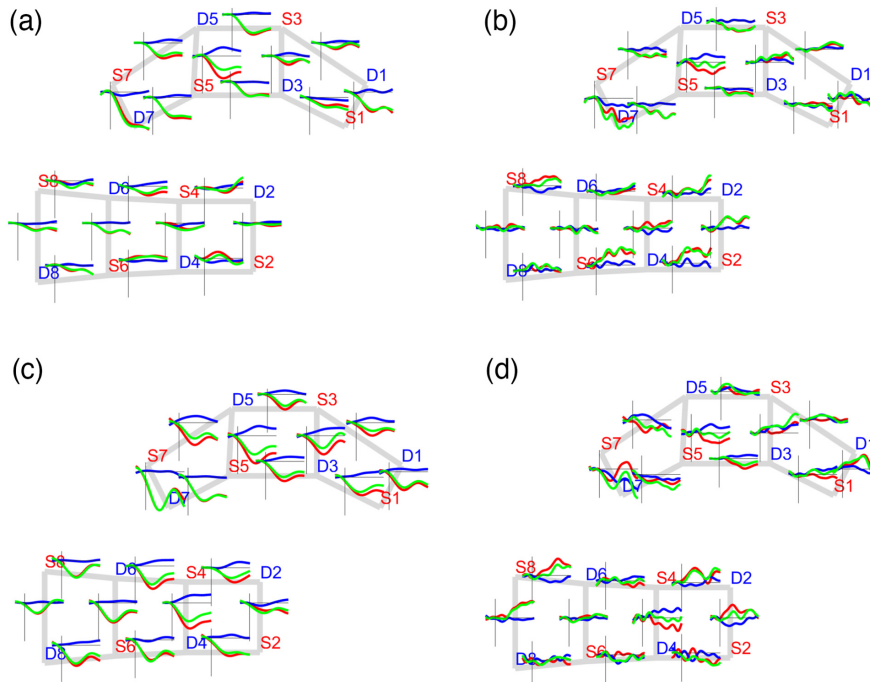


**Fig. 4** Global block-averaged response for sham (a) before and (b) after and active (c) before and (d) after applying the global signal regression to remove the global physiological effects of pain punctate stimulation (punctate). HbO<sub>2</sub>, HbR, and HbT signals are shown in red, blue, and green, respectively.

exhibited an anticorrelated temporal profile in contrast to those from the primary motor and somatosensory regions.

Figure 5 shows the block-averaged hemodynamic temporal profile at the group level for the thermal and punctate pain stimuli at the beginning of the treatment. Different cases of activation and negative activation patterns arose from the pain-evoked responses on both thermal and punctate stimuli. Activation responses are defined as an HbO<sub>2</sub> increase concomitant to an HbR decrease pattern, and negative activation responses show the opposite behavior, that is, an HbO<sub>2</sub> decrease simultaneous with an HbR increase.

With regards to the thermal stimulation type, a considerable set of channels on the primary motor and somatosensory regions showed activation patterns (sham group: S8-D8, S8-D6, S4-D6, S6-D4, and S2-D2; active group: S4-D6, S4-D2, S4-D4, S2-D2, and S6-D4), whereas channels over the PFC exhibited a negative activation response (sham group: S5-D5, S5-D3, S3-D5, and S1-D3; active group: S5-D5, S3-D3, and S1-D3).

With respect to the punctate stimulation, the sham group exhibited more activated channels covering the primary motor and somatosensory regions than the active group (sham: S8-D6, S4-D4, S2-D2, S6-D4, and S2-D4; active: S8-D6, S4-D2, S8-D8, and S2-D2). A similar number of negative activation cases were found on both the sham (S7-D5, S5-D5, and S5-S7) and active (S5-D7, S5-D5, and S5-D3) groups over the PFC region. In contrast, we observed a set of channels with opposite responses to the previous ones, that is, with an activation profile on the PFC and a negative activation response on the primary motor and sensorimotor regions. However, the number of those cases was small, and it was also investigated during the functional connectivity analysis. In general, the activation versus negative activation cases suggested an anticorrelated relationship between PFC and the primary motor and sensorimotor areas that was quantified by connectivity analysis.

### 3.3 Functional Connectivity

Functional connectivity among channels was quantified by computing a correlation between the HbO<sub>2</sub>, HbR, and HbT time series considering the blocks of stimulation periods. At the scan level,

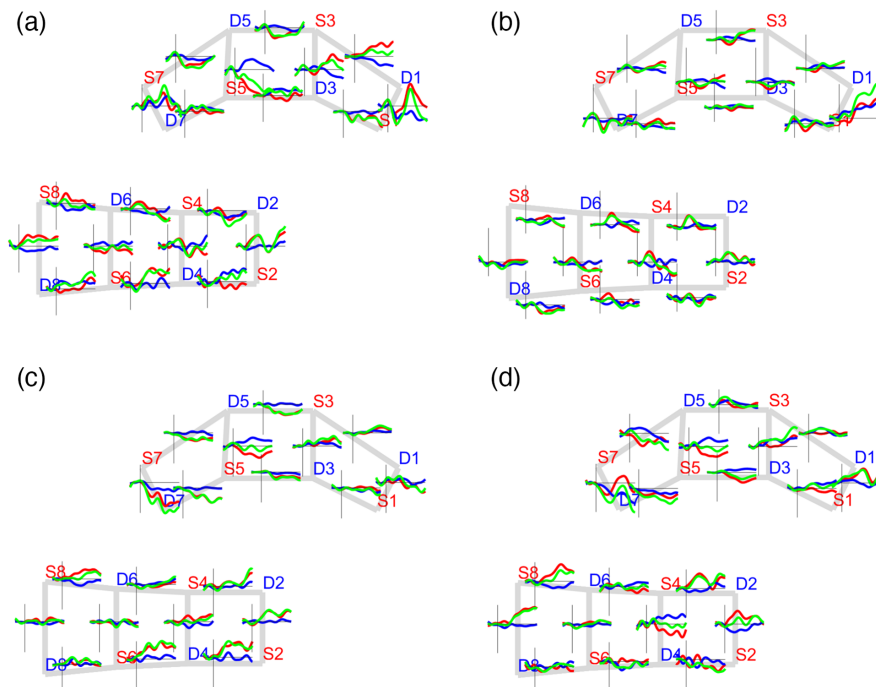


**Fig. 5** Block-averaged group-level response. The average hemodynamic response of pain stimulation during baseline (week 1). Thermal stimuli: (a) sham and (b) active; punctate stimuli (c) sham and (d) active. HbO<sub>2</sub>, HbR, and HbT signals are shown in red, blue, and green, respectively.

we obtained 743 connectivity networks, and at the group level we computed a set of 48 connectivity networks (#stimuli  $\times$  #groups  $\times$  #weeks  $\times$  #Hb types;  $2 \times 2 \times 4 \times 3$ ). The DSI metric was calculated considering only their significant connections ( $q$ -value  $< 0.05$ ). Then we based our analysis only on the HbT results due to the low HbO<sub>2</sub> – HbR symmetry value (mean = 0.02 and std = 0.01). Figure S3 in the [Supplementary Material](#) shows the DSI results for all connectivity networks at the scan level, and Figs. S1 and S2 in the [Supplementary Material](#) present the group-level HbT connectivity maps (across stimuli, groups, and weeks) and contrasts maps (week 2 to week 0), respectively.

Because we focused our analysis on the variation of functional connectivity strength, we present the functional connectivity models as connectivity matrices. In a connectivity matrix, rows and columns represent the fNIRS channels and the elements  $c_{i,j}$  represent the  $R$  coefficient value between the channels  $i$  and  $j$ . Note that this representation does not disentangle the directionality of the relationship, but only its strength. Because we did not focus on the directionality of the existing relationships, all of the resulting connectivity matrices are symmetric.

### 3.4 Thermal Stimulation

In Fig. 6, we present the HbT connectivity matrices derived from group-level analysis. For each matrix, we show the connectivity matrix and the estimated probability densities. We observed a high-positive intraconnectivity in the PFC and M1\_S1 regions in every session for both active and sham groups, as depicted in the first and second rows in Fig. 6 and Fig. S1 in the [Supplementary Material](#). Notably, we found a negative between-regions connectivity. The positive correlation among neighboring channels denotes a localized hemodynamic response, suggesting a modularity organization of the investigated brain regions, whereas the anticorrelated connections exhibit the cooperation between the PFC and primary motor and sensorimotor regions. In addition to the regional organization analysis, we computed the similarity of the connectivity models between groups based on the distributions of the  $R$ -values computed from each model. Table 1 lists the  $H$ -distances describing the longitudinal changes across weeks.

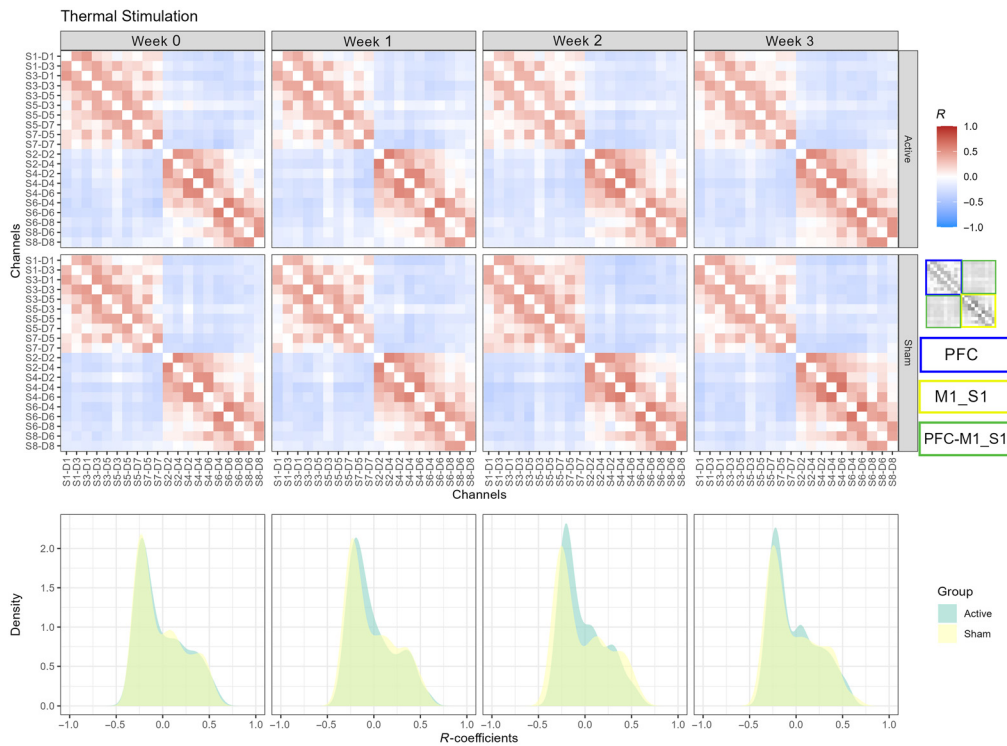


**Fig. 6** Group-level connectivity models of thermal stimulation. Color-coded correlation values for active (first row) and sham (second row) groups across sessions (columns 1 to 4). PFC, M1\_S1, and PFC-M1\_S1 regions are indicated by the blue, yellow, and green rectangles. The estimated probability densities of the active and sham groups are shown across sessions (bottom row).

**Table 1** Hellinger distances between sham and active correlation distributions for the HbT connectivity networks.  $H(A, B) = 0$  expresses identical distributions. Maximum differences between distributions across weeks are indicated in bold.

	Thermal	Punctate
Week 0	0.0250	0.0366
Week 1	0.0678	0.0833
Week 2	<b>0.1254</b>	<b>0.1215</b>
Week 3	0.0661	0.0627

The minimum distance between the densities was observed at week 0 with  $H = 0.0250$ , whereas the maximum separation was observed in week 2 ( $H = 0.1254$ ) (Fig. 6, bottom row). The low  $H$ -distance found at baseline denotes that the intra- and interregional connectivity in both groups exhibits high similar connectivity strength in response to the thermal stimulation at the beginning of the treatment. On the other hand, the maximum  $H$ -distance was found in week 2, suggesting the time point with the maximum effect of tDCS treatment. Additionally, important changes can be observed in the density shapes. For the sham group during week 2, the shape shows a more bimodal profile due to a decrease in the density around correlation values near zero, which indicates that some of the weak connections improved their strength. In terms of the network organization, it may be caused by the increasing modularity pattern in the M1\_S1 area from week 0 to week 2 [Fig. 6 (second row, M1\_S1 area, week 0 versus week 2); Fig. S1 (first row, column 3) in the [Supplementary Material](#)]. Additionally, we observed an increase in the interregional PFC-M1\_S1 negative connections from week 0 to week 2 [Fig. S1 (first row, columns 1 and 3) in the [Supplementary Material](#)]. This increment is confirmed by the statistical contrast map from week 2 to week 0 shown in Fig. S2 (first row, column 1) in the [Supplementary Material](#).

On the contrary, the opposite effects were observed for the active group. The increase in the density around zero correlation values suggests that some of the functional links weaken their correlation. This reduced effect in connectivity could be mostly observed in the intraregional connectivity of PFC [Fig. 6 (first row, columns 1 and 3); Fig. S1 (second row, columns 1 and 3) in the [Supplementary Material](#)]. The decrease in PFC connectivity was also captured by the contrast map shown in Fig. S2 (first row, column 2, PFC area) in the [Supplementary Material](#).

To investigate the interregional connectivity, we applied a threshold of  $|R| \geq 0.3$  (where  $|\cdot|$  is the absolute value) to the statistically significant functional links ( $q$ -value  $< 0.05$ ). We selected the value of 0.3 because it effectively removes the weak connections in the intraregional connectivity while keeping the interregion links. Figure S4 in the [Supplementary Material](#) illustrates the  $R$ -values of the connections along with the statistical significance before and after applying the  $|R| \geq 0.3$  threshold. Then we obtained the mean correlation and node degree within and between the PFC and M1\_S1 regions. Table 2 summarizes the statistical comparison between the sham and active groups for every connectivity model at the subnetwork level. At the beginning of the treatment, no statistically significant differences were found. We found significant

**Table 2** Comparison between groups across weeks for thermal stimulation. Correlation and degree values computed from subnetwork analysis. Statistically significant ( $p < 0.05$ ) correlation and degree values are indicated in bold.

Session	Subnetwork	Active	Sham	$p$ -value
Week 0	M1_S1 degree	21.87 (6.66)	22.06 (9.05)	0.86
	M1_S1 correlation	0.15 (0.14)	0.13 (0.19)	0.87
	PFC degree	20.00 (10.00)	21.50 (9.50)	0.58
	PFC correlation	0.12 (0.17)	0.10 (0.14)	0.42
	PFC–M1_S1 degree	39.00 (21.50)	46.00 (23.50)	0.29
	PFC–M1_S1 correlation	-0.15 (0.14)	-0.16 (0.15)	0.91
Week 1	M1_S1 degree	19.50 (12.00)	21.00 (10.00)	0.44
	M1_S1 correlation	0.13 (0.17)	0.16 (0.20)	0.46
	PFC degree	20.00 (9.00)	21.00 (10.00)	0.22
	PFC correlation	0.11 (0.09)	0.12 (0.15)	0.54
	PFC–M1_S1 degree	39.00 (18.00)	39.00 (22.00)	0.22
	PFC–M1_S1 correlation	<b>-0.13 (0.10)</b>	<b>-0.15 (0.11)</b>	<b>0.04</b>
Week 2	M1_S1 degree	20.00 (8.00)	19.50 (12.00)	0.92
	M1_S1 correlation	0.15 (0.09)	0.15 (0.15)	0.91
	PFC degree	<b>17.00 (8.00)</b>	<b>20.00 (10.00)</b>	<b>&lt;0.01</b>
	PFC correlation	<b>0.09 (0.11)</b>	<b>0.15 (0.17)</b>	<b>&lt;0.01</b>
	PFC–M1_S1 degree	<b>37.00 (18.00)</b>	<b>40.00 (24.00)</b>	<b>0.01</b>
	PFC–M1_S1 correlation	<b>-0.13 (0.10)</b>	<b>-0.16 (0.14)</b>	<b>0.01</b>
Week 3	M1_S1 degree	21.61 (7.92)	22.68 (8.12)	0.33
	M1_S1 correlation	0.16 (0.13)	0.16 (0.18)	0.81
	PFC degree	21.00 (7.00)	20.00 (9.00)	0.23
	PFC correlation	0.11 (0.14)	0.11 (0.12)	0.44
	PFC–M1_S1 degree	40.00 (17.00)	43.00 (23.00)	0.15
	PFC–M1_S1 correlation	-0.14 (0.09)	-0.17 (0.15)	0.26

differences between the sham and active groups in both week 1 and week 2. Only the interregion connectivity network (PFC-M1\_S1) exhibited differences between groups during week 1 in terms of correlation. On the other hand, significant differences were found in the PFC intra- and interconnectivity (PFC-M1\_S1) subnetworks for both correlation and degree metrics. No significant differences between the active and sham groups in correlation or degree metrics were found in the last week of the treatment.

### 3.5 Mechanical Punctate Stimulation

As in the thermal stimulation, a clear positive and negative statistical association was observed in the intra- and interregional brain connectivity, respectively. In general, the M1 and S1 areas exhibited more organized correlated responses for both the sham and active groups than the associations in the PFC (Fig. 7, first and second rows). Additionally, a decrease in the positive correlations was observed in the PFC area for the active group between week 0 and week 2 (Fig. 7, first row, columns 1 and 3), confirmed by their statistical contrast (week 2 to week 0) shown in Fig. S2 (last row columns 1 and 3) and Fig. S2 (second row column 2) in the [Supplementary Material](#). Moreover, an increment in the negative interregional PFC-M1\_S1 connections was observed in the sham group between weeks 0 and 2 (Fig. 7 second row, columns 1 and 3) and was also captured by their statistical contrast [Fig. S1 (third row, columns 1 and 3); Fig. S2 (second row, column 1) in the [Supplementary Material](#)]. In terms of the density of the correlations, a high overlap is observed between the sham and active groups at the baseline (Fig. 7, last row, first column) with a Hellinger distance of 0.0366. For week 1, the separation between groups increased for the positive and negative correlations; however, in week 2, the distance seemed to be larger for the negative associations but not for the positive correlations (Fig. 7, last row, second and third columns). Finally, the distance between densities started to decrease between groups during week 3. The evolution of the correlations from the sham group

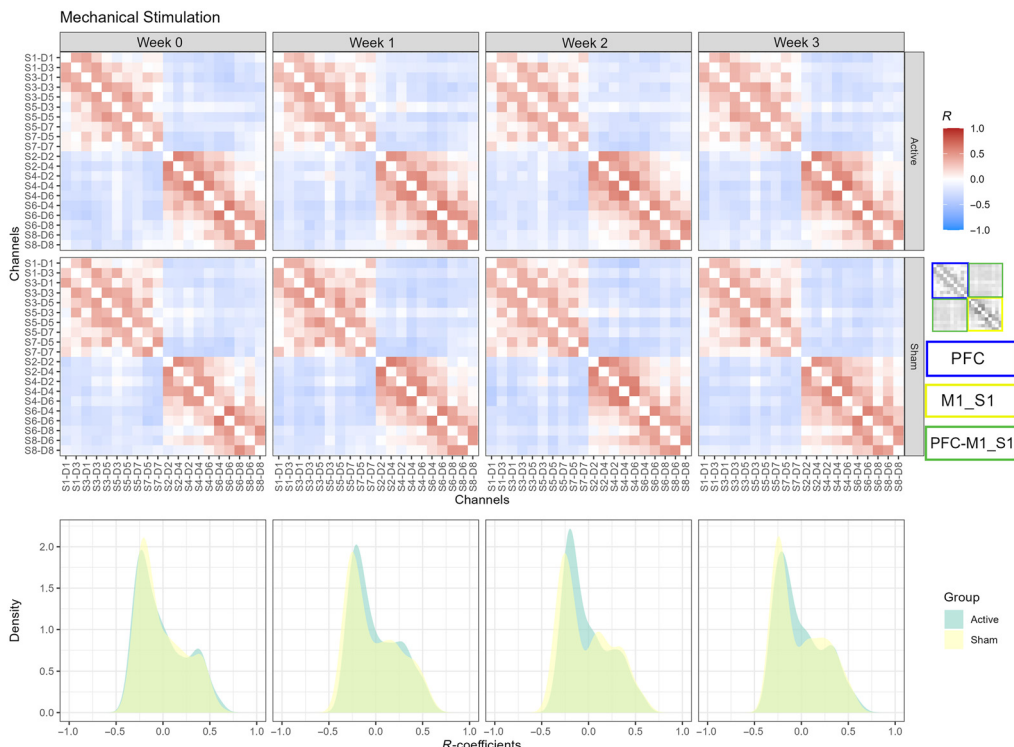


**Fig. 7** Group-level connectivity models of mechanical punctate stimulation. Color-coded correlation values for active (first row) and sham (second row) groups across sessions (columns 1 to 4). PFC, M1\_S1, and PFC-M1\_S1 regions are indicated by the blue, yellow, and green rectangles. The estimated probability densities of the active and sham groups are shown across sessions (bottom row).

showed that, in week 2, the peaks for positive correlations became more evident, suggesting a decrease in weak positive connections (close to zero correlations). Also from week 2, the density of positive correlations for both the sham and active groups started to overlap again, as at the beginning of the treatment. This suggests that, for the punctate pain stimulation, one important difference between groups was captured by the interregional brain connectivity, which exhibited mostly negative correlations.

Table 3 presents the comparison between groups across weeks for the punctate pain stimulation at the subnetwork level (correlation and degree values). We applied the same thresholding procedure ( $|R| \geq 0.3$ ) as in the subnetwork analysis. No statistical differences were found at the baseline between the sham and active groups for any subnetwork. However, we found statistically significant differences between the sham and active groups during week 1 for PFC intraregion and PFC-M1\_S1 interregion connectivity in the correlation and degree domains.

**Table 3** Comparison between groups across weeks for thermal stimulation. Correlation and degree values computed from subnetwork analysis. Statistically significant ( $p < 0.05$ ) correlation and degree values are indicated in bold.

	Subnetwork	Active	Sham	<i>p</i> -value
Week 0	M1_S1 degree	22.21 (9.23)	20.78 (9.94)	0.36
	M1_S1 correlation	0.18 (0.21)	0.12 (0.17)	0.21
	PFC degree	23.00 (8.00)	21.00 (11.00)	0.40
	PFC correlation	0.10 (0.12)	0.09 (0.11)	0.87
	PFC–M1_S1 degree	41.00 (30.00)	36.00 (32.00)	0.40
	PFC–M1_S1 correlation	−0.12 (0.17)	−0.12 (0.16)	0.26
Week 1	M1_S1 degree	24.00 (11.00)	21.50 (11.50)	0.07
	M1_S1 correlation	0.17 (0.20)	0.14 (0.18)	0.25
	<b>PFC degree</b>	<b>20.00 (7.00)</b>	<b>22.00 (5.00)</b>	<b>&lt;0.01</b>
	<b>PFC correlation</b>	<b>0.09 (0.13)</b>	<b>0.16 (0.15)</b>	<b>0.03</b>
	<b>PFC–M1_S1 degree</b>	<b>37.50 (25.00)</b>	<b>45.00 (23.00)</b>	<b>&lt;0.01</b>
	<b>PFC–M1_S1 correlation</b>	<b>−0.13 (0.12)</b>	<b>−0.17 (0.17)</b>	<b>0.01</b>
Week 2	M1_S1 degree	23.00 (13.00)	21.00 (16.00)	0.62
	M1_S1 correlation	0.17 (0.17)	0.14 (0.19)	0.46
	PFC degree	19.00 (7.00)	20.00 (11.00)	0.13
	PFC correlation	0.09 (0.09)	0.10 (0.11)	0.10
	PFC–M1_S1 degree	39.00 (22.00)	38.00 (31.00)	0.23
	PFC–M1_S1 correlation	−0.14 (0.13)	−0.15 (0.20)	0.16
Week 3	M1_S1 degree	22.00 (8.00)	21.50 (11.00)	0.60
	M1_S1 correlation	0.18 (0.14)	0.17 (0.14)	0.84
	PFC degree	19.50 (7.50)	18.50 (11.00)	0.38
	PFC correlation	0.10 (0.11)	0.10 (0.10)	0.80
	PFC–M1_S1 degree	40.00 (18.50)	44.00 (23.00)	0.26
	PFC–M1_S1 correlation	−0.14 (0.10)	−0.17 (0.15)	0.13

## 4 Discussion

In this study, we investigated the offline (poststimulation) effects of tDCS therapy on brain connectivity patterns associated with pain stimulation. Using fNIRS, our study monitored the brain hemodynamic responses following a self-administered 3-week tDCS therapy in older adults suffering from knee OA. Previously, our group investigated the use of alternative (nonpharmacological) treatments for pain management in chronic knee pain cohorts.<sup>11,13–15,41–43</sup> Our results showed changes in the connectivity at inter- and intraregional levels between the tDCS active and sham groups across weeks based on two metrics (i.e., correlation and average node degree), tracing the changes in the circuitry associated with punctate and thermal pain stimulation.

Functional responses during pain stimulation have been explored using different neuroimaging modalities.<sup>19</sup> Moreover, the use of tDCS has been previously investigated in pain management<sup>64–66</sup> and in combination with fNIRS.<sup>20</sup> The tDCS offline effects can last, in some cases, several days after the end of a tDCS session,<sup>67,68</sup> so here we report the induced changes by tDCS on functional connectivity in response to pain management during a longitudinal tDCS treatment of 15 sessions over 3 weeks and compare them against a sham tDCS therapy.

Throughout the entire experimental activity, we observed average hemodynamic responses (without the global systemic components) in agreement with the literature that associated the sympathetic skin response observed in pain-induced studies.<sup>34</sup> Also, we found concomitant decrease–increase responses in HbO<sub>2</sub> – HbR on channels covering PFC, whereas the opposite increase–decrease HbO<sub>2</sub> – HbR changes were found in M1 and S1 regions. These hemodynamic patterns have been previously reported in studies for detecting brain responses associated with thermal,<sup>21,23,30,69</sup> mechanical,<sup>70</sup> and electrical<sup>34,35</sup> pain stimulation. Hemodynamic responses to pain stimulation have been observed in cortical and subcortical regions, such as insular, primary, and secondary somatosensory (S1 and S2) cortices, anterior cingulate cortex (ACC), supplementary motor area cortices, and PFC (Bas 10, 45–47) region.<sup>18</sup> Although the functional connectivity of the mechanisms of pain may include associated processes (because pain experience can trigger concomitant processes, such as cognitive, anticipatory, emotional, and cognitive, among others), the maximum similarity value (measured by the Hellinger distance) was found between the tDCS active and sham groups at the baseline (week 0) for both stimulation types (see Table 1), whereas the minimum similarity between the active and sham connectivity networks was found during week 2. Considering the active group, weeks 1 and 3 exhibited similar Hellinger distances to the baseline values. In terms of correlation and average node degree, no statistically significant differences were found in week 0 between the active and sham groups for thermal or punctate stimulation types. With regards to thermal stimulation, we found a significant difference between the tDCS active and sham groups in weeks 1 and 2 (see Table 2), with the maximum effect of the tDCS therapy in week 2. Specifically, we found statistically significant differences in PFC-M1\_S1 on week 1 and PFC and PFC-M1\_S1 networks on week 2. In the case of the punctate stimulation, PFC and PFC-M1\_S1 networks exhibited significantly different patterns between groups in week 1 with a major effect on the number of functional connection than the connectivity strength, which has been observed in patients with hip and knee OA.<sup>71,72</sup>

We observed greater PFC average node degree and correlation values for the tDCS sham group. The PFC network from the sham group exhibited not only more functional connections but also a higher correlation among its nodes. The PFC, specifically BA 10, has been associated with an accelerated deoxygenated activity observed during nociceptive processing.<sup>32,34,73</sup> Also, it has been shown that PFC plays a role in the inhibited connectivity exhibited by the default mode network during cognitive processing,<sup>74</sup> which can be caused due to the role of BA 10 in attentional processes, such as switching focus or paying attention to pain.<sup>75</sup> Contrary to the sham tDCS, the active tDCS therapy reflected weak connectivity in PFC when dealing with pain management, which can be an indication of a weaker attentional process to pain.<sup>76,77</sup>

For the M1 and S1 regions, we observed a decrease in the (negative) connectivity strength and the number of connections for the active tDCS group. The stronger (positive) correlation and the greater number of links in the sham tDCS group can be translated into a more interacting interregion connectivity between the PFC and the M1 and S1 regions for dealing with the pain

experience. Several positive and negative coactivations between BA 10 and other brain regions, such as S1, S2, ACC, the insular cortex, dorsolateral PFC, ventrolateral PFC, premotor area, and subcortical structures such as the thalamus and striatum, have been reported in the literature.<sup>38</sup> Also the existence of different networks associated with stronger connectivity values in response to acupuncture stimulation has been shown.<sup>26</sup> Additionally, the existence of a negative correlation among different brain regions, including M1, S1, and PFC, has been observed in clinical dental pain settings using fNIRS<sup>21</sup> and in OA patients with MRI,<sup>78</sup> which supports the negative associations that we found in the interregional network connectivity.

Our results should be interpreted considering the following limitations. First, the tDCS treatment was applied in a home-based self-administered fashion, which may cause variation in the levels of efficacy across subjects. To reduce such potential variations, the participants were properly trained in the use of the tDCS device at the baseline and remotely supervised at each stimulation session by trained research staff to ensure the correct technique. Second, short separation channels were not included in the fNIRS probe due to inherent technical features of the fNIRS device used in this study (i.e., optodes could not be placed at a distance of <30 mm). However, we included a mean global systemic regression step to minimize the presence of systemic noise. Third, after the data quality assessment, we remove a subset of recordings instead of removing channels. Unlike functional studies in which every channel is associated with an activation metric, connectivity analysis always requires pairs of channels to estimate their association. Hence, we avoided pruning individual channels and opted to remove noisy scans in their entirety to obtain homogenous connectivity matrices across subjects. Considering that the large sample size ( $n = 120$ ) yielded a total of 799 recordings, the exclusion of a small subset of poor-quality recordings (56 scans or 7% of total) did not compromise the objective of this study. Finally, the fNIRS cap was carefully fitted utilizing anatomical landmarks (such as the nasion, inion, and preauricular points) as spatial references to maximize the repeatability of the optode placement. We also utilized a 3D digitizer (Polhemus Patriot) to acquire the spatial coordinates of all optodes and anatomical landmarks in 115 subjects. However, the digitization task could only be trusted for 97 subjects due to intermittent electromagnetic noise affecting the digitizer readings in our experimental facility. Notwithstanding this issue, trustworthy digital placements showed that the placement could be repeated within a few millimeters (median = 12.2 mm, IQR = 9.5 to 15.2 mm), as illustrated in Fig. S5 in the [Supplementary Material](#).

Despite these limitations, we believe that our findings provide avenues for future research studies on pain-related brain function. Our results suggest that the use of a tDCS therapy produces large-scale neuronal changes that can be captured by a functional connectivity analysis based on fNIRS. Also active and sham tDCS treatments were associated with distinguishable hemodynamic responses to pain stimulation. Finally, tDCS-derived connectivity changes could be related to the efficacy of the therapy in modulating the neural pain circuitry during nociception in knee OA patients.

## 5 Conclusion

We have investigated the effect of tDCS therapy in a pain-evoked experience at the brain connectivity level using fNIRS. We have found different longitudinal brain connectivity patterns between active tDCS therapy for pain management and sham tDCS in 120 participants across three weeks of therapy. Our results confirmed a decrease in connectivity in PFC and S1 and M1 regions after the first and second weeks of therapy for punctate and thermal pain stimulation, which contrasted with an increase in connectivity relations and strength shown by the sham tDCS group. The contrast may be associated with the tDCS therapy that promotes the modulation of PFC, S1, and M1 in the pain experience of participants. These results open the door for new investigations in the context of pain management, such as the refinement of tDCS parameters for individualized treatment.

## Disclosures

All authors have no conflicts of interest to declare.

## Acknowledgments

S.M.H. and L.P. would like to acknowledge the support of the National Science Foundation (Grant Nos. CNS 1650536 and 2137255) and I/UCRC for Building Reliable Advances and Innovation in Neurotechnology. LP also acknowledges the U.S. Fulbright Scholar Program and the Fulbright Spain Commission for sponsoring his stay at the Basque Center on Cognition, Brain and Language. The research reported in this publication was supported by the National Institute of Nursing Research of the National Institutes of Health (Award No. R15NR018050).

## Code, Data, and Materials Availability

The MATLAB scripts and functions used to process the dataset and analyze the results reported in this paper utilized the functionality of the QT-NIRS, Homer2, and NIRS Brain AnalyzIR toolboxes and can be found in Refs. 53, 79, and 80. The datasets generated and/or analyzed during the current study are available from the corresponding author upon reasonable request.

## References

1. I. J. Wallace et al., “Knee osteoarthritis has doubled in prevalence since the mid-20<sup>th</sup> century,” *Proc. Natl. Acad. Sci. U. S. A.* **114**(35), 9332–9336 (2017).
2. B. R. Deshpande et al., “Number of persons with symptomatic knee osteoarthritis in the US: impact of race and ethnicity, age, sex, and obesity,” *Arthritis Care Res. (Hoboken)* **68**(12), 1743–1750 (2016).
3. N. Cristina de Oliveira et al., “Lifestyle and pain in women with knee osteoarthritis,” *Am. J. Lifestyle Med.* **13**(6), 606–610 (2017).
4. P. Welsch et al., “Opioids for chronic osteoarthritis pain: an updated systematic review and meta-analysis of efficacy, tolerability and safety in randomized placebo-controlled studies of at least 4 weeks double-blind duration,” *Eur. J. Pain* **24**(4), 685–703 (2020).
5. E. E. Krebs et al., “Effect of opioid vs nonopioid medications on pain-related function in patients with chronic back pain or hip or knee osteoarthritis pain: the SPACE randomized clinical trial,” *JAMA* **319**(9), 872–882 (2018).
6. M. Bikson et al., “Safety of transcranial direct current stimulation: evidence based update 2016,” *Brain Stimul.* **9**(5), 641–661 (2016).
7. F. Mori et al., “Effects of anodal transcranial direct current stimulation on chronic neuropathic pain in patients with multiple sclerosis,” *J. Pain* **11**(5), 436–442 (2010).
8. M. Simis et al., “Investigation of central nervous system dysfunction in chronic pelvic pain using magnetic resonance spectroscopy and noninvasive brain stimulation,” *Pain Pract.* **15**(5), 423–432 (2015).
9. K. Pacheco-Barrios et al., “Methods and strategies of tDCS for the treatment of pain: current status and future directions,” *Expert Rev. Med. Devices* **17**(9), 879–898 (2020).
10. G. Martorella et al., “Self-administered transcranial direct current stimulation for pain in older adults with knee osteoarthritis: a randomized controlled study,” *Brain Stimul.* **15**(4), 902–909 (2022).
11. H. Ahn et al., “Bayesian analysis of the effect of transcranial direct current stimulation on experimental pain sensitivity in older adults with knee osteoarthritis: randomized sham-controlled pilot clinical study,” *J. Pain Res.* **11**, 2071–2082 (2018).
12. G. Martorella et al., “Efficacy of home-based transcranial direct current stimulation on experimental pain sensitivity in older adults with knee osteoarthritis: a randomized, sham-controlled clinical trial,” *J. Clin. Med.* **11**(17), 5209 (2022).
13. L. Pollonini, H. Miao, and H. Ahn, “Longitudinal effect of transcranial direct current stimulation on knee osteoarthritis patients measured by functional infrared spectroscopy: a pilot study,” *Neurophotonics* **7**(2), 025004 (2020).
14. L. Pollonini et al., “Functional near-infrared spectroscopy to assess central pain responses in a nonpharmacologic treatment trial of osteoarthritis,” *J. Neuroimaging* **30**(6), 808–814 (2020).

15. H. Ahn et al., “Efficacy of combining home-based transcranial direct current stimulation with mindfulness-based meditation for pain in older adults with knee osteoarthritis: a randomized controlled pilot study,” *J. Clin. Neurosci.* **70**, 140–145 (2019).
16. N. M. Lindsay et al., “Brain circuits for pain and its treatment,” *Sci. Transl. Med.* **13**(619), eabj7360 (2021).
17. G. D. Iannetti and A. Mouraux, “From the neuromatrix to the pain matrix (and back),” *Exp. Brain Res.* **205**(1), 1–12 (2010).
18. R. Peyron, B. Laurent, and L. García-Larrea, “Functional imaging of brain responses to pain. A review and meta-analysis (2000),” *Neurophysiol. Clin.* **30**(5), 263–288 (2000).
19. R. Peyron and C. Fauchon, “Functional imaging of pain,” *Revue Neurol.* **175**(1–2), 38–45 (2019).
20. R. Patel et al., “Systematic review of combined functional near-infrared spectroscopy and transcranial direct-current stimulation studies,” *Neurophotonics* **7**(2), 020901 (2020).
21. X. Hu et al., “Brain functional changes before, during, and after clinical pain,” *J. Dent. Res.* **97**(5), 523–529 (2018).
22. X. S. Hu et al., “Feasibility of a real-time clinical augmented reality and artificial intelligence framework for pain detection and localization from the brain,” *J. Med. Internet Res.* **21**(6), e13594 (2019).
23. A. J. Racek et al., “Different brain responses to pain and its expectation in the dentalchair,” *J. Dent. Res.* **94**(7), 998 (2015).
24. C. Gélinas et al., “Toward a new approach for the detection of pain in adult patients undergoing cardiac surgery: near-infrared spectroscopy—a pilot study,” *Hear. Lung J. Acute Crit. Care* **39**(6), 485–493 (2010).
25. B. D. Kussman et al., “Capturing pain in the cortex during general anesthesia: near infrared spectroscopy measures in patients undergoing catheter ablation of arrhythmias,” *PLoS One* **11**(7), e0158975 (2016).
26. R. F. Rojas et al., “Cortical network response to acupuncture and the effect of the Hegu point: an fNIRS study,” *Sensors* **19**(2), 394 (2019).
27. Z. Barati, I. Zakeri, and K. Pourrezaei, “Functional near-infrared spectroscopy study on tonic pain activation by cold pressor test,” *Neurophotonics* **4**(1), 015004 (2017).
28. L. Becerra et al., “Diffuse optical tomography of pain and tactile stimulation: activation in cortical sensory and emotional systems,” *Neuroimage* **41**(2), 252–259 (2008).
29. K. S. Hong et al., “Classification of somatosensory cortex activities using fNIRS,” *Behav. Brain Res.* **333**, 225–234 (2017).
30. R. Fernandez Rojas, X. Huang, and K. L. Ou, “A machine learning approach for the identification of a biomarker of human pain using fNIRS,” *Sci. Rep.* **9**, 5645 (2019).
31. M. Bartocci et al., “Pain activates cortical areas in the preterm newborn brain,” *Pain* **122**(1–2), 109–117 (2006).
32. K. Peng et al., “Morphine attenuates fNIRS signal associated with painful stimuli in the medial frontopolar cortex (medial BA 10),” *Front. Hum. Neurosci.* **12**, 394 (2018).
33. R. Re et al., “Cerebral cortex activation mapping upon electrical muscle stimulation by 32-channel time-domain functional near-infrared spectroscopy,” *Adv. Exp. Med. Biol.* **789**, 441–447 (2013).
34. M. A. Yücel et al., “Specificity of hemodynamic brain responses to painful stimuli: a functional near-infrared spectroscopy study,” *Sci. Rep.* **5**, 9469 (2015).
35. K. Peng et al., “Using prerecorded hemodynamic response functions in detecting prefrontal pain response: a functional near-infrared spectroscopy study,” *Neurophotonics* **5**(1), 011018 (2017).
36. C. M. Aasted et al., “Frontal lobe hemodynamic responses to painful stimulation: a potential brain marker of nociception,” *PLoS One* **11**(11), e0165226 (2016).
37. X. S. Hu, T. D. Nascimento, and A. F. DaSilva, “Shedding light on pain for the clinic: a comprehensive review of using functional near-infrared spectroscopy to monitor its process in the brain,” *Pain* **162**(12), 2805–2820 (2021).
38. K. Peng et al., “Brodmann area 10: collating, integrating and high level processing of nociception and pain,” *Prog. Neurobiol.* **161**, 1–22 (2018).

39. M. Hall et al., “Pain induced changes in brain oxyhemoglobin: a systematic review and meta-analysis of functional NIRS studies,” *Pain Med.* **22**(6), 1399–1410 (2021).
40. K. Kodama et al., “Analgesic effects of compression at trigger points are associated with reduction of frontal polar cortical activity as well as functional connectivity between the frontal polar area and insula in patients with chronic low back pain: a randomized trial,” *Front. Syst. Neurosci.* **13**, 68 (2020).
41. H. Ahn et al., “Feasibility and efficacy of remotely supervised cranial electrical stimulation for pain in older adults with knee osteoarthritis: a randomized controlled pilot study,” *J. Clin. Neurosci.* **77**, 128–133 (2020).
42. H. Ahn et al., “Efficacy of transcranial direct current stimulation over primary motor cortex (anode) and contralateral supraorbital area (cathode) on clinical pain severity and mobility performance in persons with knee osteoarthritis: an experimenter- and participant-blinded, randomized, sham-controlled pilot clinical study,” *Brain Stimul.* **10**(5), 902–909 (2017).
43. H. Ahn et al., “Home-based self-administered transcranial direct current stimulation in older adults with knee osteoarthritis pain: an open-label study,” *J. Clin. Neurosci.* **66**, 61–65 (2019).
44. R. Altman et al., “Development of criteria for the classification and reporting of osteoarthritis: classification of osteoarthritis of the knee,” *Arthritis Rheum.* **29**(8), 1039–1049 (1986).
45. F. Scholkmann et al., “How to detect and reduce movement artifacts in near-infrared imaging using moving standard deviation and spline interpolation,” *Physiol. Meas.* **31**(5), 649 (2010).
46. S. Montero Hernandez and L. Pollonini, “NIRSpot: a tool for quality assessment of fNIRS scans,” in *Biophotonics Congr.: Biomed. Opt. 2020*, p. BM2C.5, The Optical Society (2020).
47. H. Santosa et al., “Characterization and correction of the false-discovery rates in resting state connectivity using functional near-infrared spectroscopy,” *J. Biomed. Opt.* **22**(5), 055002 (2017).
48. J. W. Barker, A. Aarabi, and T. J. Huppert, “Autoregressive model based algorithm for correcting motion and serially correlated errors in fNIRS,” *Biomed. Opt. Express* **4**(8), 1366 (2013).
49. H. Santosa et al., “Quantitative comparison of correction techniques for removing systemic physiological signal in functional near-infrared spectroscopy studies,” *Neurophotonics* **7**(3), 035009 (2020).
50. T. T. Liu, A. Nalci, and M. Falahpour, “The global signal in fMRI: nuisance or information?,” *Neuroimage* **150**, 213–229 (2017).
51. P. Laska, H. Bortfeld, and T. J. Huppert, “Correction of global physiology in resting-state functional near-infrared spectroscopy,” *Neurophotonics* **9**(3), 035003 (2022).
52. Y. Zhang et al., “Eigenvector-based spatial filtering for reduction of physiological interference in diffuse optical imaging,” *J. Biomed. Opt.* **10**(1), 011014 (2005).
53. <https://github.com/lpollonini/qt-nirs>.
54. H. Santosa et al., “The NIRS brain AnalyzIR toolbox,” *Algorithms* **11**(5), 73 (2018).
55. T. J. Huppert et al., “HomER: a review of time-series analysis methods for near-infrared spectroscopy of the brain,” *Appl. Opt.* **48**(10), D280–D298 (2009).
56. A. M. Bastos and J. M. Schoffelen, “A tutorial review of functional connectivity analysis methods and their interpretational pitfalls,” *Front. Syst. Neurosci.* **9**, 175 (2016).
57. O. Sporns, *Networks of the Brain*, MIT Press, Cambridge, Massachusetts (2011).
58. S. Montero-Hernandez et al., “Estimating functional connectivity symmetry between oxy- and deoxy-haemoglobin: implications for fNIRS connectivity analysis,” *Algorithms* **11**(5), 70 (2018).
59. H. Jeffreys, “An invariant form for the prior probability in estimation problems,” *Proc. R. Soc. Lond. A. Math. Phys. Sci.* **186**(1007), 453–461 (1946).
60. J. K. Chung et al., “Measures of distance between probability distributions,” *J. Math. Anal. Appl.* **138**(1), 280–292 (1989).
61. M. Rubinov and O. Sporns, “Complex network measures of brain connectivity: uses and interpretations,” *Neuroimage* **52**(3), 1059–1069 (2010).

62. G. Marrelec and P. Fransson, "Assessing the influence of different ROI selection strategies on functional connectivity analyses of fMRI data acquired during steady-state conditions," *PloS One* **6**(4), e14788 (2011).
63. W. S. Sohn et al., "Influence of ROI selection on resting functional connectivity: an individualized approach for resting fMRI analysis," *Front. Neurosci.* **9**, 280 (2015).
64. F. Fregni et al., "A sham-controlled, phase II trial of transcranial direct current stimulation for the treatment of central pain in traumatic spinal cord injury," *Pain* **122**(1–2), 197–209 (2006).
65. B. W. Fenton et al., "A preliminary study of transcranial direct current stimulation for the treatment of refractory chronic pelvic pain," *Brain Stimul.* **2**(2), 103–107 (2009).
66. A. J. Fagerlund, O. A. Hansen, and P. M. Aslaksen, "Transcranial direct current stimulation as a treatment for patients with fibromyalgia: a randomized controlled trial," *Pain* **156**(1), 62–71 (2015).
67. K. T. Jones, F. Gözenman, and M. E. Berryhill, "The strategy and motivational influences on the beneficial effect of neurostimulation: a tDCS and fNIRS study," *Neuroimage* **105**, 238–247 (2015).
68. P. Besson et al., "Concurrent anodal transcranial direct-current stimulation and motor task to influence sensorimotor cortex activation," *Brain Res.* **1710**, 181–187 (2019).
69. L. Becerra et al., "Diffuse optical tomography activation in the somatosensory cortex: specific activation by painful vs. non-painful thermal stimuli," *PloS One* **4**(11), e8016 (2009).
70. L. Holper et al., "Physiological effects of mechanical pain stimulation at the lower back measured by functional near-infrared spectroscopy and capnography," *J. Integr. Neurosci.* **13**(1), 121–142 (2014).
71. M. N. Baliki et al., "A preliminary fMRI study of analgesic treatment in chronic back pain and knee osteoarthritis," *Mol. Pain* **4**, 47 (2008).
72. E. L. Parks et al., "Brain activity for chronic knee osteoarthritis: dissociating evoked pain from spontaneous pain," *Eur. J. Pain* **15**(8), 843.e1–843.e14 (2011).
73. L. Becerra et al., "Brain measures of nociception using near-infrared spectroscopy in patients undergoing routine screening colonoscopy," *Pain* **157**(4), 840–848 (2016).
74. M. D. Fox et al., "The human brain is intrinsically organized into dynamic, anticorrelated functional networks," *Proc. Natl. Acad. Sci. U. S. A.* **102**(27), 9673–9678 (2005).
75. P. W. Burgess, I. Dumontheil, and S. J. Gilbert, "The gateway hypothesis of rostral prefrontal cortex (area 10) function," *Trends Cogn. Sci.* **11**(7), 290–298 (2007).
76. R. Peyron et al., "Haemodynamic brain responses to acute pain in humans: sensory and attentional networks," *Brain* **122**(9), 1765–1780 (1999).
77. M. N. Baliki et al., "Beyond feeling: chronic pain hurts the brain, disrupting the default-mode network dynamics," *J. Neurosci.* **28**(6), 1398–1403 (2008).
78. M. N. Baliki et al., "Brain morphological signatures for chronic pain," *PloS One* **6**(10), e26010 (2011).
79. <http://openfnirs.org/software/homer/>.
80. <https://github.com/huppertt/nirs-toolbox>.

**Samuel Montero-Hernandez** is a postdoctoral fellow at the University of Houston. His research is focused on the design of algorithms for data analysis and causal discovery using functional near-infrared spectroscopy (fNIRS) modality. He possesses comprehensive experience in a range of areas, such as functional and effective brain connectivity analysis, data quality assurance, and probabilistic graphical models.

**Luca Pollonini** is an associate professor at the University of Houston, Texas, United States, and a visiting researcher at Basque Center on Cognition, Brain and Language, San Sebastian, Spain. His research is focused on the development of innovative instruments, methods, and applications for measuring hemodynamics and oxygenation in brain and other tissues using fNIRS and diffusion optical imaging.

**Lindsey Park** graduated from Louisiana State University with her BS degree in animal science. She has five years of clinical research and project coordinator experience. Her background in clinical research consists of projects aimed at enhancing the lives of older adults with pain.

**Geraldine Martorella** is a nurse scientist with established expertise in pain management. Her program of research aims to prevent and manage chronic pain using various nonpharmacological approaches targeting biopsychosocial risk and protective factors to improve the well-being of older adults with chronic conditions. Her experience as a clinical nurse specialist informs her research which integrates patients' and clinicians' perspectives to enhance the clinical relevance and uptake of innovative pain management interventions.

**Hongyu Miao** is a biostatistician and data scientist. He is an established expert in clinical trial, statistical learning, network analysis, time series, and big complex data with applications in digital health, mental health, pain management, neural development and disorders, and infectious diseases. By integrating engineering technologies and artificial intelligence, he has been actively developing innovative methodologies and medical interventions for public health and precision medicine.

**Kenneth B. Mathis** is a faculty in the Department of Orthopedic Surgery of McGovern Medical School at the University of Texas Health Science Center at Houston. Certified by the American Board of Orthopedic Surgery, he specializes in total joint reconstruction. He is a member of several professional organizations including the American Academy of Orthopedic Surgeons, the Texas Orthopedic Association, and the Houston Orthopedic Society.

**Hyochol Ahn** aims to enhance health and independence in vulnerable populations using innovative technologies to optimize pain and symptom management. His combined nursing, medicine, and computer engineering expertise uniquely positions him to address critical gaps in research on brain mechanisms underlying pain and other chronic symptoms and to deliver the nonpharmacological intervention to improve pain and symptom management.